

Article

## Phase Energy Determined from Stress and Electric-Field-Induced Phase Transformations in [011]<sub>C</sub> Cut 0.24PIN-PMN-PT Single Crystals

Dorinamaria Carka, John A. Gallagher and Christopher S. Lynch \*

Department of Mechanical and Aerospace Engineering, University of California Los Angeles, 420 Westwood Plaza, Los Angeles, CA 90095, USA; E-Mails: carkad@ucla.edu (D.C.); gallagherj@ucla.edu (J.A.G.)

\* Author to whom correspondence should be addressed; E-Mail: cslynch@seas.ucla.edu; Tel.: +1-310-825-7660.

Received: 8 May 2014; in revised form: 15 July 2014 / Accepted: 5 August 2014 /

Published: 19 August 2014

---

**Abstract:** The effect of composition and temperature on the large field behavior of [011]<sub>C</sub> cut and poled ( $d_{32}$ -mode) rhombohedral relaxor ferroelectric 0.24PIN-(1- $x$ )PMN- $x$ PT single crystals was characterized under electromechanical loading and the relative phase energy determined. The electric field and stress induced polarization and strain response and field dependent material properties are reported for two concentrations of lead titanate (PT), with one PT concentration closer to the morphotropic phase boundary, at low and high temperature. A thermodynamic analysis to determine the relative energy levels of the rhombohedral and orthorhombic phases is based on the path integration of the measured data to determine external work done to drive the phase transition. The effect of heat generated by irreversible strain and electric displacement increments (hysteresis in the phase transformation) was removed from the work done during the loading cycle and the relative Helmholtz free energy density levels of the phases was determined.

**Keywords:** relaxor piezoelectric; phase transformation; thermodynamics

---

### 1. Introduction

Ternary lead indium niobate-lead magnesium niobate-lead titanate,  $x\text{Pb}(\text{In}_{1/2}\text{Nb}_{1/2})\text{O}_3-(1-x-y)\text{Pb}(\text{Mg}_{1/3}\text{Nb}_{2/3})\text{O}_3-y\text{PbTiO}_3$  (PIN-PMN-PT) single crystals have been developed with the goal

of expanding the thermal, mechanical, and electrical operating ranges of relaxor ferroelectrics while reducing the temperature dependence of the material coefficients. Compared to binary lead magnesium niobate-lead titanate,  $(1-x)\text{Pb}(\text{Mg}_{1/3}\text{Nb}_{2/3})\text{O}_3-x\text{PbTiO}_3$  (PMN- $x$ PT,  $x = 0.28-0.33$ ), which has a limited operating range, PIN-PMN-PT exhibits an increased coercive field ( $E_C$ : PIN-PMN-PT up to 0.7 MV/m, PMN-PT~0.25 MV/m), depoling temperature ( $T_{R/T}$ : PIN-PMN-PT up to 137 °C, PMN-PT < 97 °C) and Curie temperature ( $T_C$ : PIN-PMN-PT up to 200 °C, PMN-PT ~ 150 °C) [1–7] while maintaining similar extraordinary piezoelectric and electromechanical properties [8–10]. The high  $T_{R/T}$ , increased thermal operating range, increased coercive field, and large piezoelectric and electromechanical properties of PIN-PMN-PT with compositions near the morphotropic phase boundary (MPB) make this relaxor single crystal useful in transducer applications such as sonar and medical ultrasound [11–14]. Recently,  $[011]_C$  relaxor ferroelectric single crystals have also been used as a platform for studying magnetoelectric heterostructures due to the anisotropic transverse piezoelectric strain response of the domain engineered crystal cut [15,16]. Miller indices are used and the notation  $[hkl]_C$  is used to indicate the directions are relative to a cubic phase.

The material properties depend on composition, orientation, domain structure, and crystallographic phase [17,18]. The compositional dependence of the stable phases at room temperature and under no applied loading for the ternary PIN-PMN-PT system is shown in Figure 1. As seen in the phase diagram  $f_{\text{PIN}}$ ,  $f_{\text{PMN}}$ , and  $f_{\text{PT}}$  correspond to the concentration of each component and low PT concentration stabilizes the rhombohedral phase ( $\text{FE}_R$ ) by reducing its Helmholtz energy density relative to other phases. The dashed line denotes the morphotropic phase boundary (MPB) that separates the rhombohedral from the tetragonal phase. The tetragonal phase is stable for higher concentrations of PT. Application of external loads above a certain threshold and in certain orientations relative to the crystal structure induces a phase transformation to a non-equilibrium phase [19–22]. Compositions of  $[011]_C$  cut and poled PMN-PT ( $d_{32}$  mode) in the ferroelectric rhombohedral phase ( $\text{FE}_R$ ) can be driven to the ferroelectric orthorhombic phase ( $\text{FE}_O$ ) by an applied uniaxial compressive stress in the  $[100]_C$  direction or by an applied electric field in the  $[011]_C$  direction [19,21,22]. Similar results were reported recently for PIN-PMN-PT [23]. The polarization reorientation is shown schematically in Figure 2. The mechanical and electrical loads shown work cooperatively to induce the transformations, *i.e.*, each provides a positive driving force for the transformation because the applied stress and electric field components shown do positive work on the strain and electric displacement change associated with the transformation. The  $\text{FE}_R$ - $\text{FE}_O$  transformation is associated with a large non-linear and hysteretic jump in strain and electric displacement and the transformation from  $\text{FE}_R$  to  $\text{FE}_O$  results in large reductions in compliance, piezoelectric, and dielectric constants [21,22]. In this work experiments were run on  $[011]_C$  cut and poled  $d_{32}$ -mode PIN-PMN-PT single crystals in the  $\text{FE}_R$  phase to characterize their large field behavior under thermal and electromechanical loading. The effects of composition and temperature on the phase transition in two PT concentrations and at two different temperatures was compared. Non-linear material behavior was observed in the electric displacement-electric field, strain-electric field and stress-strain diagrams. The hysteretic jump is analyzed and discussed in some detail.

**Figure 1.** Room temperature phase diagram for PIN-PMN-PT [24]. The morphotropic phase boundary (MPB) between the ferroelectric rhombohedral ( $FE_R$ ) and ferroelectric tetragonal (T) phases is depicted by the dashed red line. The black dots show the approximate compositions used in this work.

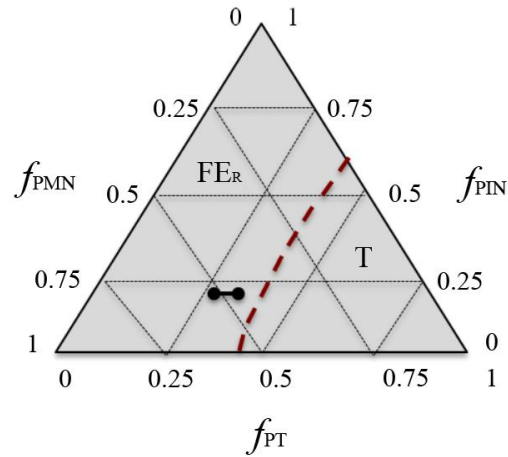
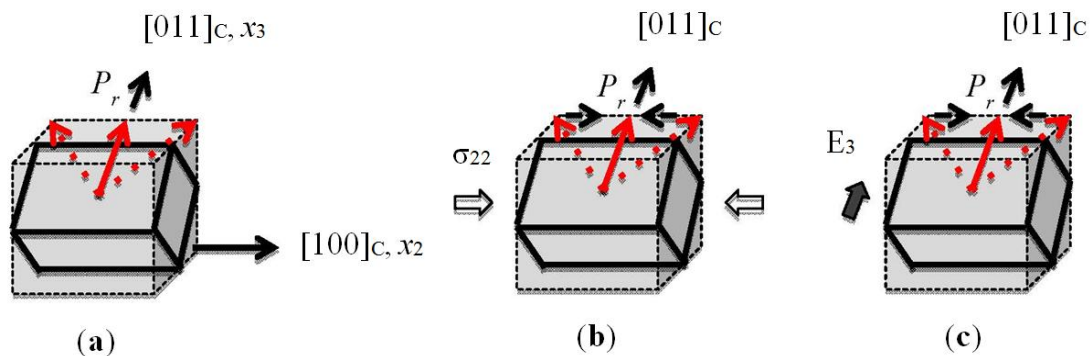


**Figure 2.** Domain states and field driven phase transformations for  $[011]_C$  cut and poled ferroelectric single crystals. (a)  $[011]_C$  cut and poled single crystals made by cutting the single crystal at a 45 degree rotation about  $[100]_C$ . Two of the  $\langle 111 \rangle$   $FE_R$  variants are populated with the volume average remanent polarization in the  $[011]_C$  direction; (b) Compressive stress ( $\sigma_{22}$ ) in the  $[100]_C$  direction induces a  $FE_R$  to  $FE_O$  phase transformation where only the  $[011]_C$  variant is populated; (c) Application of electric field ( $E_3$ ) in the  $[011]_C$  direction induces the same  $FE_R$ - $FE_O$  transformation.



Non-linear behavior of ferroelectric materials can be described using a thermodynamics based approach outlined by Devonshire [25]. This approach was extended in the phenomenological Landau-Devonshire theory that has been used to explain a range of phase transformations and nonlinearities in the material behavior [26]. These phase transformations display jumps in the Helmholtz free energy and discontinuities in the derivatives of the Gibbs free energy and can be described using higher-order Devonshire theory. In this work, path integrals of experimental electric field—electric displacement and stress—strain curves were used to calculate the Helmholtz energy. Such an approach has previously been used to describe the multi-field transformation behavior of PMN-0.32PT and PZN-0.045PT [27].

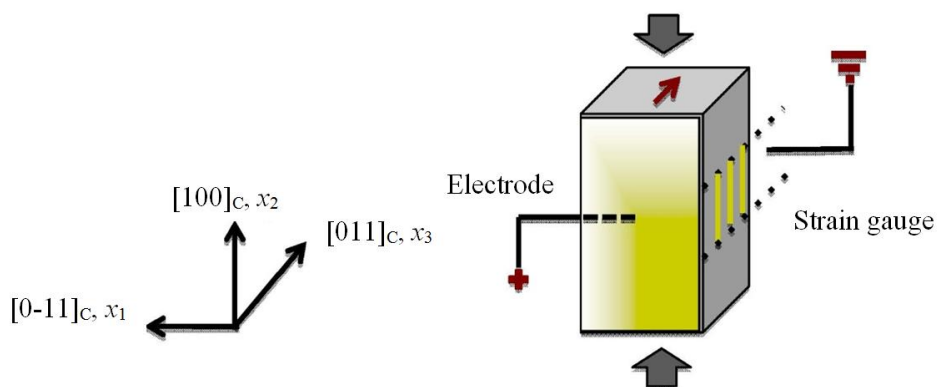
The thermodynamics based analysis was used to determine the effect of PT concentration on the energy associated with the transformation. Path integrals were used to determine the external work done by electrical and mechanical loading at two temperatures to induce the  $FE_R$ - $FE_O$  phase transformation. The heat generated during the loading cycle was removed from the external work by assuming equal parts of heat are generated by irreversible strain and electric displacement increments during the forward and reverse transformation. Although the phase transformation displays asymmetry, the assumption that half of the dissipation occurs on the forward transformation and half on the reverse transformation does not affect the results appreciably. The relative Helmholtz energy density levels of the phases was determined by fitting the linear behavior of the material on the rhombohedral and orthorhombic phases. The results are discussed in terms of the Landau-Devonshire theory for phase transformations.

## 2. Experimental Approach

### 2.1. Specimen Preparation

Different specimens of relative dimensions of  $4 \times 4 \times 12 \text{ mm}^3$  were cut of 0.24PIN-PMN-PT relaxor ferroelectric single crystals were cut with the long axis taken along the  $[001]_C$  direction and with faces perpendicular to the  $[011]_C$  direction as shown in Figure 2a. The PT concentrations place the high PT closer to, and the low PT, farther from the morphotropic phase boundary (MPB). In  $d_{32}$ -mode the (011) faces are electroded. This way, an electric field,  $E_3$ , is produced between the electrodes accompanied by an induced  $D_3$  electric displacement and a corresponding  $\epsilon_{22}$  strain in the  $[001]_C$  direction. Electrodes were formed by gold sputtering and leads were attached to the electrodes using silver epoxy. Strain gauges were placed on non-electroded faces on opposite sides towards the center of the specimen. The  $d_{32}$ -mode specimen assembly is shown in Figure 3.

**Figure 3.** Bulk single crystal stack assembly for the  $d_{32}$ -mode  $[011]_C$  cut direction. The red arrows denote the electric field loading direction (volume average initial remnant polarization is in the same direction) while the grey arrows denote the stress loading direction.



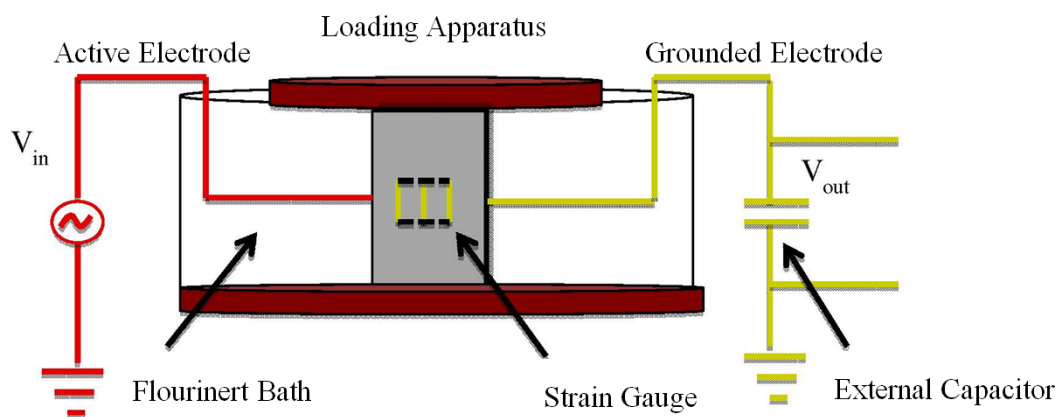
### 2.2. Experimental Arrangement

The thermo-electro-mechanical loading arrangement and the specimen placement are shown in Figure 4. The mechanical and electrical loading were applied using a screw driven load frame and a

high voltage power supply. The arrangement of the  $[011]_C$  cut specimen was such that the electric field was applied along the 4 mm thickness in the  $[011]_C$  direction and the mechanical loading along the 12 mm axis in the  $[001]_C$  direction so that increasing electric field  $E_3$  and increasing compressive stress  $\sigma_{22}$  produce an increase in  $D_3$  and a decrease in  $\epsilon_{22}$  as diagrammed in Figure 2a–c. The specimens were submerged in a flourinert bath to provide electrical insulation. A heating strip and thermocouple were placed within the flourinert bath to control the temperature.

Strain was measured with a Wheatstone bridge strain gauge amplifier in quarter bridge configuration and electric displacement was measured with a modified Sawyer Tower circuit. An electrometer was used to read the voltage across this capacitor,  $V_{out}$ . Electric displacement was calculated by dividing the charge by the electrode area. Electric field was calculated by dividing the applied voltage,  $V_{in}$ , by the specimen thickness. A series of electrical and mechanical cycles were applied to the specimens using a triangle wave profile. The maximum loading amplitude for each test was chosen to induce full  $FE_R$  to  $FE_O$  transformation. For both PT compositions of 0.30 and 0.32 the electric field was cycled at 0.2 Hz with no mechanical preload and stress was cycled at a rate of 0.625 MPa/s. This procedure was repeated at temperatures of 25 °C, 35 °C, 45 °C, 55 °C and 65 °C. The 0.30 PT composition did not fully transform at 25 °C at an electric field of 2 MV/m. The data for 35 °C and 65 °C are presented here and subjected to the thermodynamic analysis.

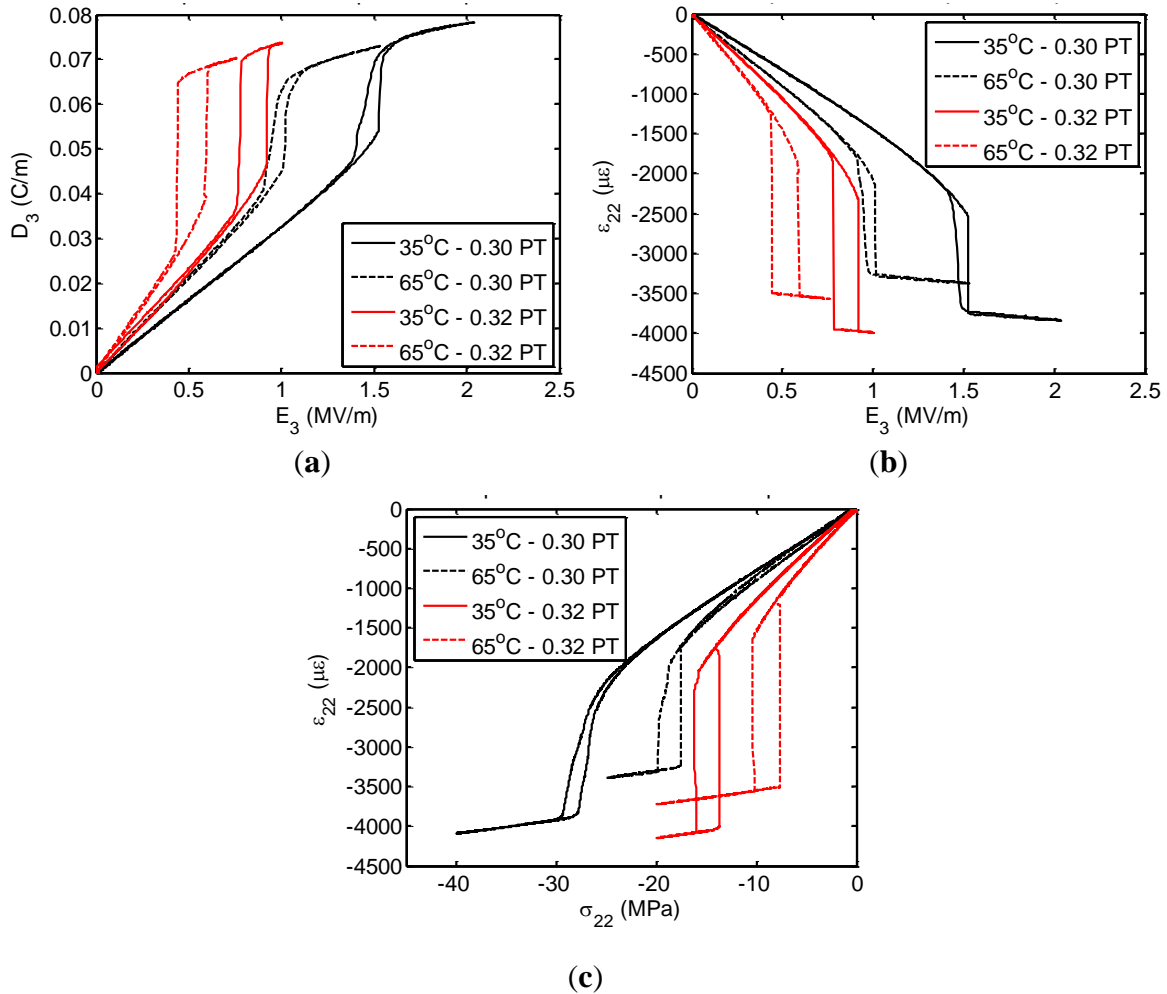
**Figure 4.** Schematic of the combined loading apparatus.



### 3. Experimental Results

The measured nonlinear electromechanical response at 35 °C and 65 °C of 0.24PIN-PMN- $x$ PT for  $x = 0.30$  and  $x = 0.32$  PT is shown in Figure 5. The electric displacement *vs.* electric field and strain *vs.* electric field response at zero applied stress are plotted in Figure 5a,b respectively. The stress *vs.* strain response at zero electric field is plotted in Figure 5c. In both the electrical and mechanical loading, as the loading is increased past a certain threshold the specimen undergoes a phase transformation. It is assumed that due to the crystal cut of the specimens and the loading direction, the secondary phase has orthorhombic symmetry resulting from the polarization rotation of the  $\langle 111 \rangle$  variants to the  $\langle 011 \rangle$  direction, an  $FE_R$  to  $FE_O$  phase transformation. The phase transformation occurs with a well-defined hysteresis in the  $D_3$ - $E_3$ ,  $\epsilon_{22}$ - $E_3$  and  $\epsilon_{22}$ - $\sigma_{22}$  diagrams, enclosed by the forward ( $FE_R$ - $FE_O$ ) reverse ( $FE_O$ - $FE_R$ ) transformation paths.

**Figure 5.** (a)  $D_3$ - $E_3$  (b)  $\varepsilon_{22}$ - $E$  and (c)  $\varepsilon_{22}$ - $\sigma_{22}$  loops for 0.24PIN-PMN- $x$ PT for two different temperatures. The black lines correspond to  $x = 0.30$  PT and the red lines to  $x = 0.32$  PT with increasing PT percentage pointing towards the MPB. The solid and dashed lines correspond to low (35 °C) and high (65 °C) bath temperature respectively.



The effect of increasing PT is evident in the electromechanical response and the phase transformation behavior as seen in Figure 5a–c. In the  $D_3$ - $E_3$  plotted data for 0.30 PT and 0.32 PT concentration at 35 °C a small offset was detected in the electric displacement upon unloading to zero electric field. It was assumed that the offset was a result of a small leakage current in the system and the data were corrected by assuming a linear resistor in parallel with the specimen with resistance equal to the offset. The phase transformation for the 0.32 PT composition occurred with a sharp jump in the strain and electric displacement and a well-defined hysteresis width. On the other hand, the 0.30 PT composition exhibited a more distributed ( $\text{FE}_R$ - $\text{FE}_O$ ) and ( $\text{FE}_O$ - $\text{FE}_R$ ) transition and a distinct transformation threshold was not as clearly deduced. For both compositions the transformation pattern persisted at higher temperatures. The 0.32 concentration of PT, closer to the MPB, shows a lower threshold for transformation under electric field and stress. The polarization and strain changes associated with the transformation are larger for the composition closer to the MPB. As the temperature is increased, the transformation threshold is reduced for both compositions. The effect of temperature on the strain and polarization jumps is similar, both decrease with increasing temperature.

The decrease in the transformation threshold with increasing PT concentration and temperature is accompanied by a change in the corresponding material properties. As it can be seen from the D<sub>3</sub>-E<sub>3</sub> loop, the  $\kappa_{33}^{\sigma}$  dielectric permittivity is larger in the composition closer to the MPB. There is a similar effect on the piezoelectric coefficient, leading to an increase of the  $d_{32}$  parameter of  $\varepsilon_{22}$ -E and of the compliance  $s_{22}^E$  of  $\varepsilon_{22}$ - $\sigma_{22}$ . Increasing the temperature led to a further increase of the dielectric and piezoelectric and compliance constants for both compositions, however the temperature dependence of the material properties is not the same for the two compositions.

The composition further from the MPB was more sensitive to the thermal loading, *i.e.*, there are larger slope changes with temperature in the FE<sub>R</sub> phase and a larger reduction in the phase transformation threshold than in the composition closer to the MPB. The material constants were deduced by fitting the corresponding measured data in the linear regimes corresponding to the rhombohedral and orthorhombic phase when saturation was achieved are presented in Table 1, together with error estimates. The phase transformation leads to a large decrease in the material dielectric, piezoelectric, and compliance constants, with the orthorhombic material constants being an order of magnitude less than the corresponding material constants of the rhombohedral phase.

**Table 1.** Fitted material properties.  $\kappa_0 = 8.855 \times 10^{-12}$  F/m is the permittivity of free space.

Fitted properties	x = 0.30 PT		x = 0.32 PT	
	35 °C	65 °C	35 °C	65 °C
	$\kappa_{33}^{\sigma}/\kappa_0$			
FE <sub>R</sub>	3260 ± 30	4573 ± 30	4320 ± 30	6381 ± 30
FE <sub>O</sub>	880 ± 30	960 ± 30	1290 ± 30	883 ± 30
	$d_{32}$ (pC/N)			
FE <sub>R</sub>	-1436 ± 30	-2022 ± 30	-2052 ± 30	-2708 ± 30
FE <sub>O</sub>	-212 ± 30	-259 ± 30	-200 ± 30	-277 ± 30
	$s_{22}^E$ (10 <sup>-12</sup> 1/Pa)			
FE <sub>R</sub>	79 ± 3	94 ± 3	113 ± 3	183 ± 3
FE <sub>O</sub>	17 ± 3	26 ± 3	16 ± 3	18 ± 3

#### 4. Thermodynamic Analysis

A thermodynamic based analysis of the data is presented in this section. It follows the analysis applied by Liu *et al.* [27] of field induced phase transformations in relaxor ferroelectric single crystals. The main points of the theory are given herein. The rate of change of internal energy in a stationary ferroelectric crystal in the absence of body forces and charges can be written in the local form as:

$$\dot{u} = \dot{w} + \dot{q} \quad (1)$$

where  $\dot{u}$  the change in internal energy density,  $\dot{q}$  the rate of heat added by external sources and  $\dot{w} = \dot{w}^m + \dot{w}^e$  the rate of work done on the body which, in the case of ferroelectric crystals, can be separated in a mechanical and an electrical part. Assuming that the elastic and electric behavior of the ferroelectric is fully described by the components of electric field  $E_i$  electric displacement  $D_i$  the components of the Cauchy stress tensor,  $\sigma_{ij}$  and the small deformation strain,  $\varepsilon_{ij}$  the incremental form of the above equation can be written as:

$$du = E_i dD_i + \sigma_{ij} d\varepsilon_{ij} + dq \quad (2)$$

For the material under consideration the electric displacement and mechanical strain can be represented by a summation of a reversible (elastic) part,  $D_i^e$  and  $\varepsilon_{ij}^e$ , and an irreversible (dissipative) part,  $D_i^r$  and  $\varepsilon_{ij}^r$  associated with the dissipation that arises during to domain wall motion and phase transformation in the material upon loading and unloading. Substitution of the additive decomposition of the strain and electric displacement increments in Equation (2) gives:

$$du = E_i dD_i^e + \sigma_{ij} d\varepsilon_{ij}^e + \underbrace{E_i dD_i^r + \sigma_{ij} d\varepsilon_{ij}^r}_{Tds} + dq \quad (3)$$

where  $T$  is the temperature and  $s$  the entropy density. Equation (3) implies that the work done by the irreversible parts of the strain and electric displacement increments contributes to the total dissipation resulting in an increase of the thermal energy in the body according to the second law of thermodynamics. Integrating Equation (2) along a loading path we have:

$$\int_A^B du = \int_A^B E_i dD_i + \int_A^B \sigma_{ij} d\varepsilon_{ij} + \int_A^B dq \Rightarrow \Delta u = \Delta w + \Delta q \quad (4)$$

Note that  $\Delta q = 0$  under adiabatic loading conditions where there is no heat transfer between the body and the surroundings, which will result in a temperature increase in the body due to dissipation. If the loading process is isothermal and under a full cycle of loading where the electric and mechanical loads return to the same point, and the loading rate is sufficiently slow that temperature gradients in the specimen can be neglected, the  $\Delta q$  term in the second part of Equation (4) represents the heat generated due to the dissipation in the material since  $\Delta u = 0$  and  $\Delta q = -\Delta w$ . Although the phase transformation itself may be adiabatic due to the transformation rate, the dissipation associated with the forward/reverse phase transformation does not change the temperature enough to affect the transformation. The specific heat is around 0.5 kJ/kg-K, the density is around 7800 kg/m<sup>3</sup> and the dissipation is around 5 kJ/m<sup>3</sup>. The temperature change in a single cycle associated with this dissipation is on the order of 0.002 degrees.

Therefore during a closed loading cycle under quasi-isothermal conditions we have:

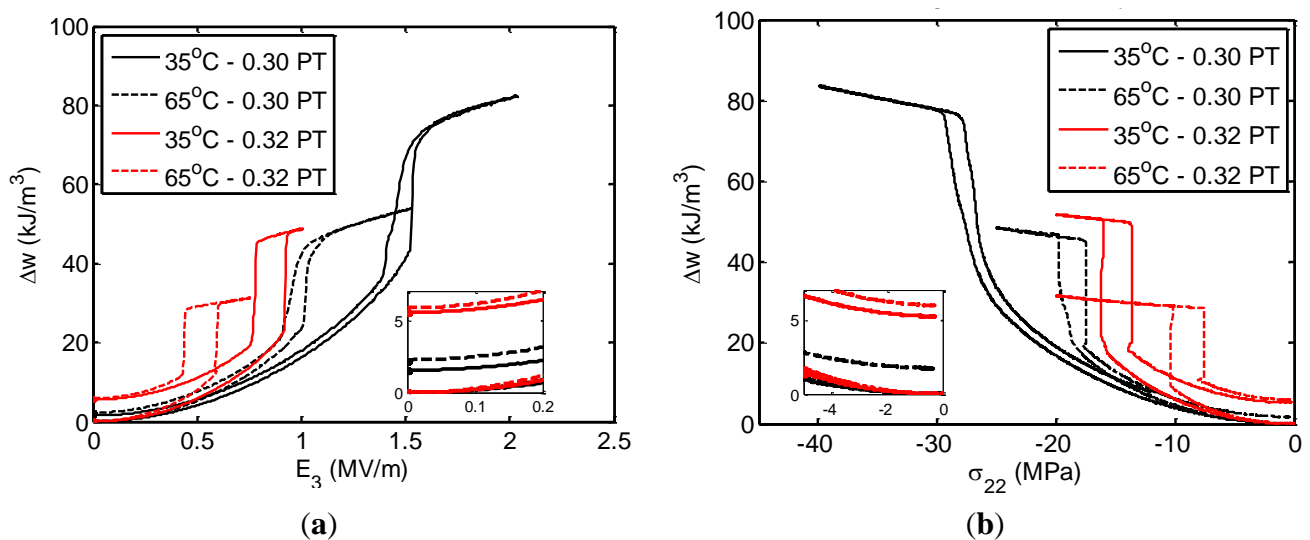
$$\oint (E_i dD_i + \sigma_{ij} d\varepsilon_{ij}) = \Delta w^e + \Delta w^m = -\Delta q \quad (5)$$

Equation (5) is applied directly to integrate measured experimental data for the mechanical and electrical loading cycles and any offset represents the heat generated due to dissipation in the material. This offset is equal to the area within the hysteresis loops. The results are shown in Figure 6.

Figure 6a shows the numerical integration results for the electric field cycle data reported in Figure 5a. Note that in this case only the electric term of the first part of Equation (5) contributes to the work done on the material. Figure 6b, represents the integrated work done on the material during the stress cycle data that was presented in Figure 5c. The inserts in Figure 6a,b are a close up of the offset of the integrated electrical and mechanical work that, as stated above, represent the heat generated due to the dissipative part of the loading. A first observation of the integrated work is that the amount of heat generated during the loading cycles is approximately 5.6 kJ/m<sup>3</sup> for the 0.32 PT, and approximately 2 kJ/m<sup>3</sup> for the 0.30 PT concentrations. The effect of temperature on the dissipation is very small, within the margin of error of the experimental data. The effect of PT concentration on the

dissipation is in accordance with the area of the hysteresis loops in  $D_3$ - $E_3$  and  $\varepsilon_{22}$ - $\sigma_{22}$  of Figure 5a,c respectively. The material with PT concentration closer to the MPB dissipates approximately twice as much energy as the material with PT concentration away from the boundary. The dissipation in the material during the phase transformation under mechanical or electrical loading is almost equal for a given composition.

**Figure 6.** Integrated work done during the (a) electric field and (b) stress loading. The insert is a close up to the amount of heat generated by the irreversible electric displacement and strain increments for the  $x = 0.30$  PT and  $x = 0.32$  PT at 35 °C and 65 °C.



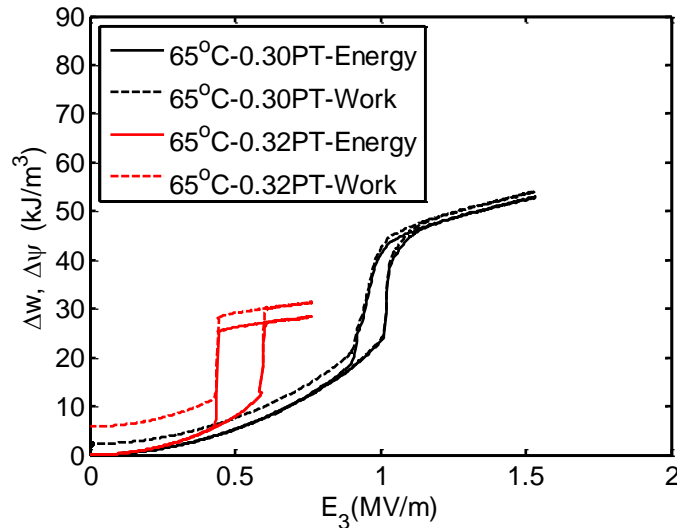
Relative changes in the Helmholtz energy levels of the rhombohedral and orthorhombic phases were determined using the results of Figure 6, obtained by applying Equation (5) to the measured experimental data. The effect of the heat generated during the loading cycles was removed by assuming that the energy dissipated during the full loading cycle can be divided into equal parts during the loading and unloading. This assumption is supported to great extent by the hysteretic paths during the loading and unloading cycles retaining similar symmetry for a given PT concentration at both temperatures. For the full loading cycle after correction for the offset associated with the dissipation, the Helmholtz free energy is given by Equation (6):

$$\int_A^B d\psi = \int_A^B (du - Tds) = \int_A^B (E_i dD_i + \sigma_{ij} d\varepsilon_{ij}) \quad (6)$$

Figure 7 shows the Helmholtz free energy after subtracting the heat generated from the work done during the electric loading cycle for the two concentrations at 35 °C. As shown and discussed in Section 3 the PT concentration has an effect on phase transformation behavior of the material. For the PT concentration closer to the MPB boundary the transformation is abrupt and the transformation threshold and polarization jump are clearly associated with a distinct field value. In this case it is assumed that the dissipation is constant with respect to the electric displacement increment and half of the dissipation takes place during the forward transformation and the other half during the reverse transformation. For the PT concentration away from the MPB, the transformation is distributed and the threshold not as clearly associated with a single distinct field value. Here it was assumed that dissipation

was distributed equally between the forward and reverse transformation paths but in this case the dissipation was taken to be linear with respect to the electric displacement increment. Applying these assumptions gives the plots shown in Figure 7, with no offset in the Helmholtz free energy upon unloading and a slight change in slope on the part corresponding to the loading and unloading of the orthorhombic phase.

**Figure 7.** Helmholtz free energy obtained by subtracting the dissipation from the external work done during the loading cycle.



Since the material behavior is linear for the parts corresponding to the  $FE_R$  phase before the forward transformation and the  $FE_O$  phase after the forward and before the reverse transformation they can be represented by the linear piezoelectric Equation (7):

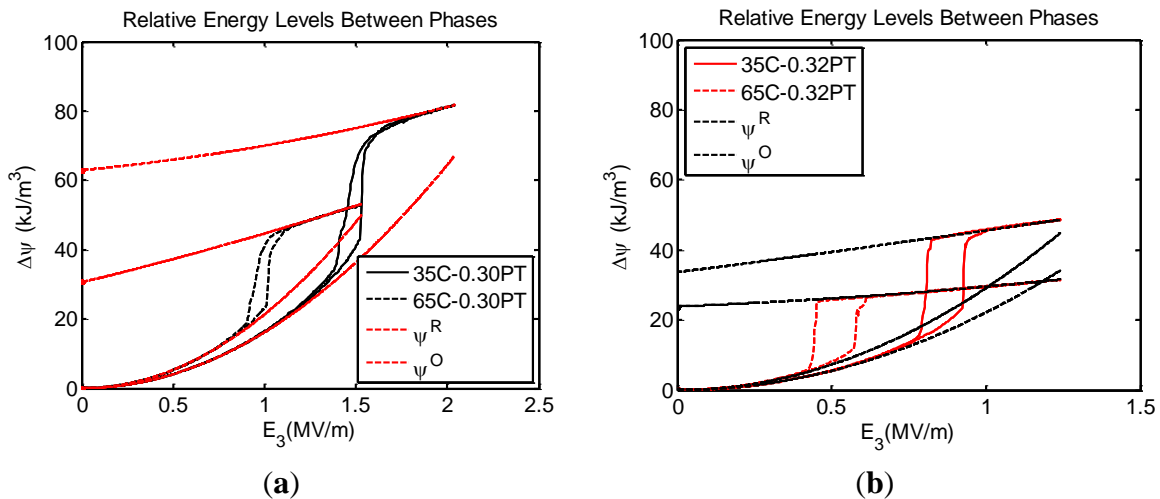
$$\begin{aligned} \epsilon_{22} - \epsilon_{22}^r &= S_{2222}^E \sigma_{22} + d_{322} E_3 \\ D_3 - D_3^r &= d_{322} \sigma_{22} + \kappa_{33}^\sigma E_3 \end{aligned} \tag{7}$$

The quadratic form of the Helmholtz free energy corresponding to the above constitutive equations is then written as:

$$\psi - \psi_0 = \frac{1}{2} S_{2222}^E \sigma_{22}^2 + d_{322} \sigma_{22} E_3 + \frac{1}{2} \kappa_{33}^\sigma E_3^2 \tag{8}$$

Here  $\psi_0$  is a reference free energy level at zero electric field and zero stress. Using the fitted data reported in Table 1 the quadratic forms of the free energy corresponding to the linear regime in the  $FE_R$  or  $FE_O$  phases are superimposed on the Helmholtz energy plots. This enables extrapolation of the energy of the  $FE_O$  phase to zero load, giving the energy difference between the phases. Figure 8 shows the relative free energy levels of the  $FE_R$  and  $FE_O$  phases for the PT concentration closer to the MPB at two different temperatures. The relative change of free energy between the phases is overall smaller for the PT concentration closer to the MPB, which implies a lower energy barrier to the transformation.

**Figure 8.** Relative free energy levels the  $FE_R$  and  $FE_O$  phases for the PT concentration closer to the MPB boundary at 35 °C and 65 °C.



## 5. Conclusions

The effect of composition on the large field response of a mode  $d_{32}$  [011] cut 0.24PIN-PMN- $x$ PT single crystal was characterized under electromechanical loading for two different temperatures. Two concentrations of PT,  $x = 0.30$  and 0.32 PT were considered. The effect of composition in both the overall phase transformation behavior and threshold field levels was discussed. The 0.32 PT concentration close to the MPB showed a sharp transformation with large jumps in strain and polarization at low electric and stress field levels. The phase transformation for the 0.30 PT concentration, away from the MPB, occurred in a more distributed fashion across a range of electric and stress fields, both of which were higher than for the 0.32 PT. Increasing the PT concentration and temperature led to an increase in the measured dielectric, piezoelectric, and compliance coefficients of the two phases. Increasing temperature caused the phase transformation to occur at lower field for both compositions.

The data were subjected to a thermodynamics analysis to obtain the relative Helmholtz free energy levels of the rhombohedral and orthorhombic phases at zero electric field and stress. Assuming isothermal conditions, the free energy was derived by numerically integrating the electromechanical work done on the material and removing the offset associated with dissipation. A quadratic form of the free energy was superposed on the linear  $FE_R$  and  $FE_O$  phases and extrapolated to zero loading. It was found that the composition closer to the MPB has a lower energy barrier between the two phases. This energy barrier decreased with temperature.

## Author Contributions

Christopher Lynch supervised the overall project and provided with guidance on the experiments, analysis and the writing of the manuscript. John Gallagher performed the experiments and Dorinamaria Carca performed the theoretical analysis and writing of the manuscript.

## Conflicts of Interest

The authors declare no conflict of interest.

## References

1. Xu, G.; Chen, K.; Yang, D.; Li, J. Growth and electrical properties of large size  $\text{Pb}(\text{In}_{1/2}\text{Nb}_{1/2})\text{O}_3\text{-Pb}(\text{Mg}_{1/3}\text{Nb}_{2/3})\text{O}_3\text{-PbTiO}_3$  crystals prepared by the vertical Bridgman technique. *Appl. Phys. Lett.* **2007**, *90*, 032901:1–032901:3.
2. Tian, J.; Han, P.; Huang, X.; Pan, H.; Carroll, J.F. Improved stability for piezoelectric crystals grown in the lead indium niobate-Lead magnesium niobate-Lead titanate system. *Appl. Phys. Lett.* **2007**, *91*, 222903:1–222903:3.
3. Tian, J.; Han, J.; Carroll, J.F.; Payne, D.A. Growth and improved properties of ternary piezoelectric single crystals in lead indium niobate-lead magnesium niobate-lead titanate system. In Proceedings of the IEEE International on Ultrasonics Symposium (IUS), Rome, Italy, 20–23 September 2009.
4. Luo, J.; Zhang, S.; Shrout, T.R. The progress update of relaxor piezoelectric single crystals. In Proceedings of the IEEE International on Ultrasonics Symposium (IUS), Rome, Italy, 20–23 September 2009.
5. Zhang, S.; Fei, L. High performance ferroelectric relaxor- $\text{PbTiO}_3$  single crystals: Status and perspective. *J. Appl. Phys.* **2012**, *111*, 031301:1–031301:50.
6. Zhang, S.; Luo, J.; Hackenberger, W.; Shrout, T.R. Characterization of  $\text{Pb}(\text{In}_{1/2}\text{Nb}_{1/2})\text{O}_3\text{-Pb}(\text{Mg}_{1/3}\text{Nb}_{2/3})\text{O}_3\text{-PbTiO}_3$  ferroelectric crystal with enhanced phase transition temperatures. *J. Appl. Phys.* **2008**, *104*, doi:10.1063/1.2978333.
7. Hosono, Y.; Yamashita, Y.; Sakamoto, H.; Ichinose, N. Dielectric and piezoelectric properties of  $\text{Pb}(\text{In}_{1/2}\text{Nb}_{1/2})\text{O}_3\text{-Pb}(\text{Mg}_{1/3}\text{Nb}_{2/3})\text{O}_3\text{-PbTiO}_3$  ternary ceramic materials near the morphotropic phase boundary. *Jpn. J. Appl. Phys. Part 1 Regul. Pap. Short Notes Rev. Pap.* **2003**, *42*, 535–538.
8. Kuwata, J.; Uchino, K.; Nomura, S. Phase transitions in the  $\text{Pb}(\text{Zn}_{1/3}\text{Nb}_{2/3})\text{O}_3\text{-PbTiO}_3$  system. *Ferroelectrics* **1981**, *37*, 579–582.
9. Kuwata, J.; Uchino, K.; Nomura, S. Dielectric and Piezoelectric Properties of  $0.91\text{Pb}(\text{Zn}_{1/3}\text{Nb}_{2/3})\text{O}_3\text{-}0.09\text{PbTiO}_3$  Single Crystals. *Jpn. J. Appl. Phys.* **1982**, *21*, doi:10.1143/JJAP.21.1298.
10. Park, S.-E.; Shrout, T.R. Ultrahigh strain and piezoelectric behavior in relaxor based ferroelectric single crystals. *J. Appl. Phys.* **1997**, *82*, 1804–1811.
11. Uchino, K. *Piezoelectric Actuators and Ultrasonic Motors*; Springer-Verlag: New York, NY, USA, 1996.
12. Park, S.E.; Shrout, T.R. Characteristics of relaxor-based piezoelectric single crystals for ultrasonic transducers. *IEEE Trans. Ultrason. Ferroelectr. Freq. Control* **1997**, *44*, 1140–1147.
13. Kobayashi, T.; Shimanuki, S.; Saitoh, S.; Yamashita, Y. Improved growth of large lead zinc niobate titanate piezoelectric single crystals for medical ultrasonic transducers. *Jpn. J. Appl. Phys. Part 1 Regul. Pap. Short Notes Rev. Pap.* **1997**, *36*, 6035–6038.
14. Shrout, T.R.; Park, S.E.; Lopath, P.D.; Meyer, R.J.; Ritter, T.A.; Shung, K.K. Innovations in piezoelectric materials for ultrasound transducers. In SPIE—The International Society for Optical Engineering, Proceedings of the Conference on Ultrasonic Transducer Engineering—Medical Imaging 1998, San Diego, CA, USA, 21 February 1998.

15. Wu, T.; Bur, A.; Zhao, P.; Mohanchandra, K.P.; Wong, K.; Wang, K.L.; Lynch, C.S.; Carman, G.P. Giant electric-field-induced reversible and permanent magnetization reorientation on magnetoelectric Ni/(011) [Pb(Mg<sub>1/3</sub>Nb<sub>2/3</sub>)O<sub>3</sub>](1-x)-[PbTiO<sub>3</sub>]x heterostructure. *Appl. Phys. Lett.* **2011**, *98*, doi:10.1063/1.3534788.
16. Liu, M.; Howe, B.M.; Grazulis, L.; Mahalingam, K.; Nan, T.; Sun, N.X.; Gail, B. Voltage-Impulse-Induced Non-Volatile Ferroelastic Switching of Ferromagnetic Resonance for Reconfigurable Magnetoelectric Microwave Devices. *Adv. Mater.* **2013**, *25*, 4886–4892.
17. Viehland, D.; Amin, A.; Li, J.F. Piezoelectric instability in <011>-oriented Pb((B1/3B2/3II)-B-I)O-3-PbTiO<sub>3</sub> crystals. *Appl. Phys. Lett.* **2001**, *79*, 1006–1008.
18. Zhao, X.Y.; Fang, B.; Cao, H.; Guo, Y.; Luo, H. Dielectric and piezoelectric performance of PMN-PT single crystals with compositions around the MPB: Influence of composition, poling field and crystal orientation. *Mater. Sci. Eng. B Solid State Mater. Adv. Technol.* **2002**, *96*, 254–262.
19. Viehland, D.; Li, J.F. An hysteretic field-induced rhombohedral to orthorhombic transformation in <110>-oriented 0.7Pb(Mg<sub>1/3</sub>Nb<sub>2/3</sub>)O<sub>3</sub>-0.3PbTiO<sub>3</sub> crystals. *J. Appl. Phys.* **2002**, *92*, 7690–7692.
20. Cross, L.E. Relaxor ferroelectrics: An overview. *Ferroelectrics* **1994**, *151*, 305–320.
21. Liu, T.; Lynch, C.S. Ferroelectric properties of [110], [001] and [111] poled relaxor single crystals: Measurements and modeling. *Acta Mater.* **2003**, *51*, 407–416.
22. McLaughlin, E.A.; Liu, T.; Lynch, C.S. Relaxor ferroelectric PMN-32%PT crystals under stress and electric field loading: I-32 mode measurements. *Acta Mater.* **2004**, *52*, 3849–3857.
23. Gallagher, J.A.; Tian, J.; Lynch, C.S. Effects of composition and temperature on the large field behavior of [011]<sub>C</sub> relaxor single crystals. *Appl. Phys. Lett.* **2014**, doi:10.1063/1.4892451.
24. Zhang, S.; Shrout, T. Relaxor-PT single crystals: Observations and developments. *IEEE Trans. Ultrason. Ferroelectr. Freq. Control* **2010**, *57*, 2138–2146.
25. Devonshire, A.F. Theory of Ferroelectrics. *Adv. Phys.* **1954**, *3*, 85–130.
26. Vanderbilt, D.; Cohen, M.H. Monoclinic and triclinic phases in higher-order Devonshire theory. *Phys. Rev. B Condens. Matter Mater. Phys.* **2001**, *63*, doi:10.1103/PhysRevB.63.094108.
27. Liu, T.; Lynch, C.S.; McLaughlin, E.A. Thermodynamics of stress and electric field induced phase transition in relaxor ferroelectric crystals. *J. Intell. Mater. Syst. Struct.* **2007**, *18*, 409–415.